Case Studies in Thermal Engineering 60 (2024) 104824

Contents lists available at ScienceDirect

Case Studies in Thermal Engineering

journal homepage: www.elsevier.com/locate/csite

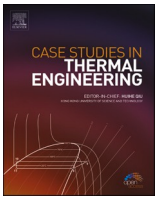

Mapping of hydrocarbon condensation onset temperature and its sensitivity analysis for Exhaust Gas Recirculation (EGR) cooler

Zhiqiang Han [a,b], Liping Luo [a], Yipeng Yao [a,b,c,*], Hai Du [b], Wei Tian [a,b], Xueshun Wu [a], Marie-Eve Duprez [c], Guy De Weireld [c]

[a] Key Laboratory of Fluid and Power Machinery, Ministry of Education, Xihua University, Chengdu, 610039, China
[b] Engineering Research Center of Ministry of Education for Intelligent Air-Ground Fusion Vehicles and Control, Xihua University, Chengdu, 610039, China
[c] Thermodynamics and Mathematical Physics Unit, Faculty of Engineering, University of Mons, 20 Place du Parc, Mons, 7000, Belgium

ARTICLE INFO

Keywords:
EGR cooler
Hydrocarbon
Condensation
Onset temperature
Sensitivity analysis

ABSTRACT

Exhaust Gas Recirculation (EGR) cooling technology is one of the key technologies of the engine to meet the Euro 7 emission standard. Nevertheless, the hydrocarbon (HC) condensation in the cooler leads to uncontrolled thermal-hydraulic performance, and the onset temperature of HC condensation is still debated, which is one of the obstacles to implementing the Euro 7 standard. Here, we first established a database of key parameters (carbon number, concentration, and pressure); then theoretically calculated the onset temperatures of various condensation types (wall condensation, heterogeneous nucleation, and homogeneous nucleation), plotted the entire map and verified its veracity; and finally, elucidated the contribution of each parameter through sensitivity analysis. The results show that (i) HC species are C12 to C25, from 25 to 1717 ppm concentrations, and pressures are from 1 to 4 bar. (ii) The map diagrams for the onset temperature of HC condensation have broad applicability and strong practicality. (iii) The temperature ranges of the onset of wall condensation, heterogeneous nucleation, and homogeneous nucleation are from 4 to 218 °C, from 1 to 209 °C, and from −6 to 195 °C, respectively. (iv) Carbon number has the most significant contribution, followed by HC concentration and pressure. The results can provide a valuable reference for more accurate EGR cooler design and management.

1. Introduction

Exhaust Gas Recirculation (EGR) cooling technology can significantly reduce the combustion temperature in internal combustion engine cylinders by dilution, thermal, and chemical effects, reducing the nitrogen oxide (NOx) emissions [1–7]. Particularly after the release of the Euro 4 standard, this technology has been widely used [8]. The Euro 7 standard, planned to be released by the European Commission before 2027, will further limit the NOx emission level [9], which puts forward the demand for higher standards of EGR cooling technology.

However, since the EGR cooling technology was proposed in the 1990s, the associated fouling problems have not been really solved to date, and it causes additional energy and economic losses [10], which is a thorny but unavoidable issue. Fouling may trigger several unfavorable results: (i) reduction of heat exchange effectiveness [11–16]; (ii) increase of pressure drop [12,17–19]; (iii) complete failure due to clogging of the cooler [19–21]. Recent studies have shown that HC condensation is one of the principal contributions in

* Corresponding author. Thermodynamics and Mathematical Physics Unit, Faculty of Engineering, University of Mons, 20 Place du Parc, Mons, 7000, Belgium.
E-mail address: yipeng.yao@umons.ac.be (Y. Yao).

https://doi.org/10.1016/j.csite.2024.104824
Received 8 May 2024; Received in revised form 7 July 2024; Accepted 10 July 2024
Available online 14 July 2024

the generation of fouling, which is manifested in three pathways (interaction with particles, homogeneous nucleation, and interaction with the fouling) and five effects (filling, removal, chemical, adhesion, and nucleation) [22]. Furthermore, HC condensation can also enhance briefly the heat transfer performance of the cooler through the released latent heat of phase change [23], several other studies have similarly confirmed that HC may promote heat transfer in some cases [24–27], but in the long run, this may induce more severe fouling. Therefore, the condensation of HC significantly affects the thermal-hydraulic performance of the EGR cooler. However, it is worth warning that all these effects are unintentional; they can change the fluid properties (temperature, flow rate, pressure, etc.) of the exhaust gas at the outlet of the cooler and can keep them out of the design values, which finally disturbs the temperature and concentration profiles in the cylinder, triggering harmful combustion and high emissions. Therefore, it is necessary to investigate the condensation characteristics of HC inside the EGR cooler.

Recently, different studies have identified parameters such as species [13,26], concentration [25,28–30] of HC, and coolant temperature [13,19,30,31] as the key factors affecting condensation, and have well elucidated their effects on the HC condensation with considerable progress. However, there are still inconsistent and even conflicting results regarding the onset temperature of HC condensation in EGR coolers. Table 1 summarizes the 16 previous studies published boundary conditions and critical results. Roughly speaking, there is a great discrepancy between the results. On one hand, researchers have suggested that the temperature at which HC can condense until 115 °C [23] or even 160 °C [25] and that homogeneous nucleation and heterogeneous nucleation can also take place at 85 °C [32]. On the other hand, some researchers have argued that HC condensation does not take place at high temperatures. Abarham et al. have suggested that in the range from 50 °C to 90 °C, HC lighter than C20 do not condense [33], and there are no HC species lighter than C22 that can condense above 80 °C [34], while Tanaka et al. suggest that HC do not condense at 80 °C to 120 °C [35]. All these results are confusing, and the difference in boundary conditions may be one of the reasons as it can make results' comparison quite difficult. But in any case, the significant difference between the boundary conditions and the results for the onset temperature of HC condensation in the EGR cooler and the lack of solid robustness of the conclusions is a notable point of debate.

Under the constraints of Euro 7 standards, EGR coolers with lower temperatures and broader operating domains are one of the feasible paths [41,42]. However, the potential negative consequences accompanying HC condensation need to be avoided. Therefore, it is necessary to find the appropriate temperature operating region under these constraints. As the condensation onset temperature is

Table 1
Summary of previous key results regarding HC condensation onset temperature in EGR cooler.

Reference	Year	Method[a]	Pressure (bar)	HC concentration (ppm)	Key result	Is map applicable?
Sluder et al. [36]	2008	Experiment	–	416~618	HC as light as C15 condenses in a cooling tube at 40 °C	Yes
Abarham et al. [33]	2009	Theory	–	259	HC less than C20 do not condense in the range from 50 °C~90 °C	Yes
Bika et al. [37]	2012	Experiment	–	250	Significant nucleation at 40 °C and below	Yes
Warey et al. [38]	2012	Theory	1.5	2~10	C15 hardly condenses at a cooling temperature of 35 °C	Yes
Abarham et al. [34]	2013	Theory	1.25	≤100	No HC species lighter than docosane can condense above 80 °C	No
Warey et al. [39]	2013	Experiment	–	250	Increased condensation nucleation detected at 40 °C	Yes
Warey et al. [39]	2013	Theory	–	42/250	HC species lighter than n-tetradecane are unlikely to condense	Yes
Tanaka et al. [35]	2016	Theory	1.01	6000~7000	The calculated condensation temperature was approximately 50 °C, which means that the gas-phase hydrocarbons do not condense in the temperature range of 80~120 °C, where the LT and HT lacquers are formed	No
Paz et al. [40]	2019	Theory	–	1030~1100	The dew temperature of eicosane (96.5 °C) is high enough to ensure condensation throughout the test in the outlet region, which is in line with the study of Warey et al. [39]	No
Razmavar and Malayeri [23]	2019	Experiment	1.01	100	Eicosane condenses at 90 °C	Yes
Razmavar and Malayeri [23]	2019	Theory	1.01	100	Eicosane begins to condense at temperatures close to 115 °C	Yes
Galindo et al. [41]	2020	Experiment	–	–	Atomization, i.e., nucleation, below 50 °C	Yes
Paz et al. [29]	2021	Theory	–	578~1265	The dew points of $C_{16}H_{34}$ at 851 ppm and 1265 ppm are 52.0 °C and 60.1 °C, respectively	No
Zhang et al. [31]	2021	Experiment	–	–	HC nucleation was more pronounced at 75 °C than at 85 °C	Yes
Li et al. [32]	2022	Experiment	–	200/450/850	HC heterogeneous nucleation and homogeneous nucleation both exist at 85 °C	Yes
Han et al. [25]	2023	Experiment	1.08	359/411/590	Condensation of HC in the cooler is almost inhibited at temperatures above 160 °C	Yes

Note: '-' is not specified; '/' is used to separate multi-values.
[a] : This method classification pertains to the acquisition of HC condensation onset temperature results, not the acquisition of metadata (pressure, carbon number, HC concentration).

the criterion to distinguish whether condensation occurs, it is a key parameter for developing the EGR cooler operation strategy. The onset temperatures of HC condensation in the EGR cooler are highly heterogeneous and even contradictory, this work aims to systematically construct a map of the onset temperatures of HC condensation over the entire operating range of the EGR cooler, which is required to have a wide range of adaptability and practicality. Specifically, this work will address the following sub-problems.

(i) What are the types of HC condensation and their discriminatory conditions?
(ii) What are the main influencing parameters and their distribution range?
(iii) What is the onset temperature of HC condensation?
(iv) What is the contribution of the influencing parameters?

Lastly, based on the study's results, a brief discussion is presented from the perspective of the onset temperature of HC condensation in the context of the new requirements of the upcoming Euro 7 standard. In conclusion, this study analyzes the global distribution of onset temperature of HC condensation for the EGR cooler and will provide new insights into the design and management of EGR coolers.

2. Methodology

2.1. Type of condensation and its determination criteria

Some studies have shown that condensation of exhaust gases typically occurs in two categories: surface condensation and bulk gas condensation [39]. Based on this, a previous work summarized in detail the three pathways of condensation in exhaust gases, namely interaction with particles, homogeneous nucleation, and interaction with the fouling [22]. Among them, the interaction with particles includes two sub pathways: (i) heterogeneous nucleation of gas-phase HC and tiny particles and (ii) condensation of gas-phase HC on the surface of particulate matter.

The saturation ratio is often used to determine whether or to what extent condensation occurs, and the saturation ratio (SR) is defined as the ratio of the partial pressure (P_v) of substance to the saturated vapor pressure (P_{sat}) of the same substance at a given temperature [43]:

$$SR = \frac{P_v}{P_{sat}(T)} \tag{1}$$

For a given HC species, partial pressure is a function of total pressure and concentration, and saturated vapor pressure is a function of temperature. Thus, the main parameters are therefore the HC species, concentration, and total pressure. The HC species, concentration, and total pressure were obtained through literature review and saturated vapor pressure are provided by. Aspen Plus® V14 provided It should be noted that only n-alkanes were considered for the HC species. To construct a broad spectrum profile of the onset temperature of HC condensation, considering as many scenarios as possible across the full operating range of the EGR cooler, this work conducted an widespread literature review to create a metadata database of the key influencing factors, with publications from sources including, but not limited to Scope, SAE, Heat Exchanger Fouling & Cleaning Conference Series [10], within the time frame from 1995 to 2024.

Theoretically, due to the cooling wall having sufficient cold and condensation sites, surface condensation at the wall can occur when the saturation ratio of HC vapors at the interface is equal to 1, whereas the other modes usually require higher saturation ratios to appear. For gas-phase HC condensation on the surface of particulate matter, we are not aware of any relevant studies investigating their saturation ratios, and due to the lack of referable data, this condensation mode is not currently considered in this paper. Considering both nucleation modes, heterogeneous nucleation is more likely to occur due to the presence of nuclei that can reduce meaningfully the minimum Gibbs free energy required for HC vapor condensation nucleation as compared to homogeneous nucleation. However, the saturation ratio for heterogeneous nucleation is not a fixed value. It is usually affected by many factors such as material, concentration, size, and shape of the particles, and the distribution is in the range from 1.3 to 2.2 [44–47]. In this paper, it is assumed that heterogeneous nucleation occurs when the saturation ratio is 1.5. Whereas homogeneous nucleation does not occur easily, and it requires saturation ratios up to 3 to 4 before it occurs [48], it is assumed in this paper that it occurs when the saturation ratio is 3. Therefore, in this paper, saturation ratios 1, 1.5, and 3 are chosen as the criteria for wall condensation, heterogeneous nucleation, and homogeneous nucleation.

It is worth stating that there are several key assumptions in this work: (i) This paper assumes that all HC in the exhaust gas are n-alkanes and does not consider iso-alkanes and HC derivatives, which are also present in the exhaust gas and do not have the same condensation characteristics as n-alkanes, with the onset temperature of HC condensation usually being slightly higher at same carbon number. (ii) This paper does not consider the actual flow conditions in the EGR cooler, which are very complex due to the presence of fins or helical ripples, and the concentration and partial pressure of HC may be highly inhomogeneous, which may also cause the actual onset temperature of HC condensation to deviate from the map. (iii) The saturation ratios of the three condensation types are theoretical values. In practice, the nature of the wall surface (roughness, hydrophilicity, material, etc.), the nature of the central nucleus (size, shape, material, etc.), and the nature of other gases (non-condensable gases) all affect HC condensation, and these interactions are very complex. Therefore, the actual onset temperature of HC condensation may differ from the map diagram, and the magnitude of this uncertainty needs to be analyzed on a case-by-case basis for further study.

2.2. Sensitivity analysis

A sensitivity analysis was conducted to elucidate the contribution of the influencing factors on the onset temperature of the HC condensation. The analysis method is the variance method of global sensitivity analysis, which can both qualitatively resolve the sequence of influence degrees of the parameters and quantify the value of the contribution rate [49–51].

The influencing factors studied in this paper consist of three parameters, *i.e.*, carbon number, concentration, and total pressure, as shown in Table 2. The range of values for each factor is derived from the survey results in Section 3.1, and the values of the four levels are equally distributed.

Orthogonal design can effectively reduce the number of calculations by uniformly combining different levels of different factors. Table 3 shows the orthogonal design and the corresponding level configurations in this study, with 16 combinations L16(4^3), where the number of occurrences of each level in the orthogonal experimental design is consistent.

Eqs. (2)–(4) allow for the calculation of the degree of influence of the parameter. The larger the sum of squares of the total deviation S, the more significant the impact of the parameter.

$$S=\sum_{i=1}^{n}(y_i-\bar{y})^2=\sum_{i=1}^{n}y_i^2-\frac{1}{n}\left(\sum_{i=1}^{n}y_i\right)^2 \tag{2}$$

Where n is the number of rows in the orthogonal table, and $\bar{y}$ is the mean.

$$S_j=\sum_{i=1}^{m}(k_i-\bar{y})^2 \tag{3}$$

Where m is the number of levels of the factor, which is 4 in this study, and k_i is the mean of the factor at the corresponding level.

The contribution ρ of factor j is:

$$\rho_j=\frac{S_j}{S}(\%) \tag{4}$$

3. Results and discussion

3.1. The distribution range of core parameters

Fig. 1 shows the carbon number distribution of HC condensed in EGR coolers from 10 studies. The large balls at the endpoints represent the upper and lower extremes of the carbon number, and the small balls are intermediate values, which were also detected or used in the corresponding papers. Overall, the distribution of carbon numbers of spans from C12 to C25. Of these, only Sluder et al. [36] measured the carbon number of HC condensates in cooling tubes using gas-chromatography-mass spectrometry (GC-MS), which showed a carbon number of C15 to C25, with peak concentrations occurring near C19 and C20; none of the other studies tested the carbon number, but assumed a specific value of carbon number as a proxy for HC. based on these considerations, C12, C16, C20, and C24 have been chosen as the representative carbon numbers to balance the need for sufficiently broad coverage and moderate gradient settings in the sensitivity analysis.

Fig. 2 shows the concentration distribution of HC in the EGR cooler, from 21 studies. Although the concentrations used in those studies differ, they are mainly distributed in two intervals: from 25 to 1717 ppm and from 3500 to 8900 ppm. The second range is not typical of engine exhaust gases and is outside the range of regular EGR operation. Those concentrations are purposely constructed as ultra-high concentrations to accelerate fouling [18] and to simulate the regeneration of diesel particulate filter (DPF) [35,53–55]. Therefore, the concentration distribution of HC in the EGR cooler ranges from 25 to 1717 ppm, which is the data band used for subsequent calculations.

Fig. 3 shows pressure distributions inside the EGR cooler, from 13 studies where both high-pressure and low-pressure stage EGRs were considered. The results show that the pressures in most studies are between 1 and 2 bar, while the high-pressure EGR often reaches 4 bar due to transient changes in operating conditions [42]. Therefore, the distribution of pressures in the EGR cooler is in the range from 1 to 4 bar, based on which the representative values of pressures chosen for the subsequent calculations in this paper are 1, 2, 3, and 4 bar, respectively.

3.2. Saturation ratio distribution map

According to Eq. (1), distribution maps of saturation ratios can be obtained for different core parameters (carbon number, concentration and pressure) at different temperatures. Fig. 4 (a) to (d) shows the distribution of the saturation ratio of C12 with

Table 2
Influencing factors and level design.

Level	Carbon number	Concentration (ppm)	Pressure (bar)
(i)	12	25	1
(ii)	16	589	2
(iii)	20	1153	3
(iv)	24	1717	4

Table 3
The orthogonal array of L16(4^3).

Program	Carbon number	Concentration (ppm)	Pressure (bar)
①	12	25	1
②	12	589	2
③	12	1153	3
④	12	1717	4
⑤	16	25	2
⑥	16	589	1
⑦	16	1153	4
⑧	16	1717	3
⑨	20	25	3
⑩	20	589	4
⑪	20	1153	1
⑫	20	1717	2
⑬	24	25	4
⑭	24	589	3
⑮	24	1153	2
⑯	24	1717	1

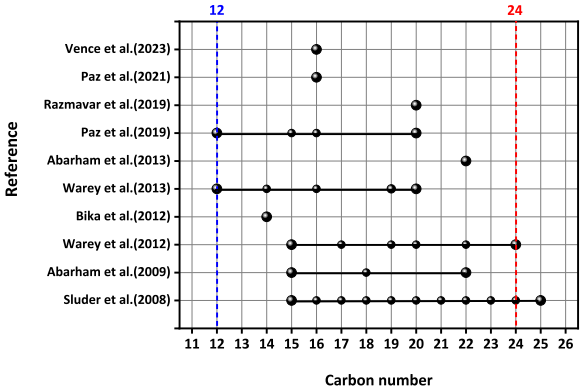

Fig. 1. Carbon number distribution database of HC condensation in EGR cooler (Reference: Sluder et al. (2008) [36]; Abarham et al. (2009) [33]; Warey et al. (2012) [38]; Bika et al. (2012) [37]; Warey et al. (2013) [39]; Abarham et al. (2013) [34]; Paz et al. (2019) [40]; Razmavar et al. (2019) [23]; Paz et al. (2021) [29]; Vence et al. (2023) [52]).

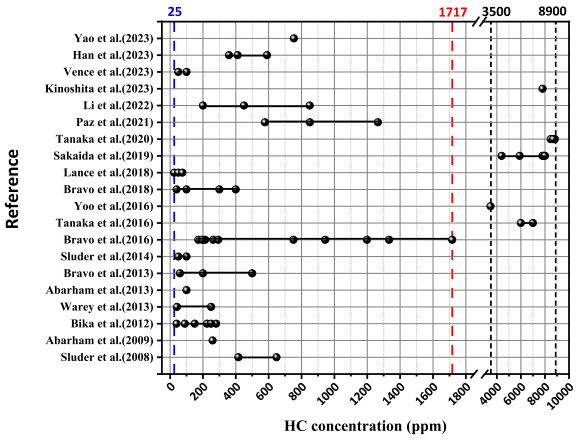

Fig. 2. HC concentration distribution database in EGR cooler (Reference: Sluder et al. (2008) [36]; Abarham et al. (2009) [33]; Bika et al. (2012) [37]; Warey et al. (2013) [39]; Abarham et al. (2013) [34]; Bravo et al. (2013) [56]; Sluder et al. (2014) [57]; Bravo et al. (2016) [58]; Tanaka et al. (2016) [35]; Yoo et al. (2016) [18]; Bravo et al. (2018) [19]; Lance et al. (2018) [30]; Sakaida et al. (2019) [53]; Tanaka et al. (2020) [54]; Paz et al. (2021) [29]; Li et al. (2022) [32]; Kinoshita et al. (2023) [55]; Vence et al. (2023) [52]; Han et al. (2023) [25]; Yao et al. (2023) [59]).

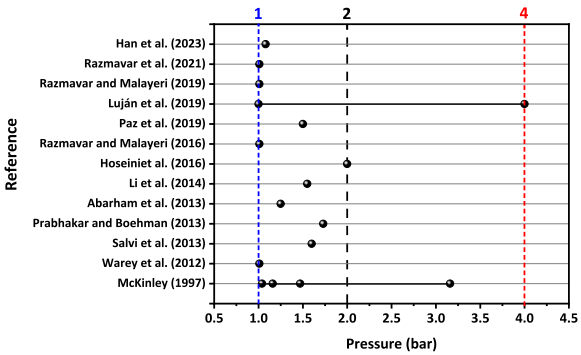

Fig. 3. Pressure distribution database in EGR cooler (Reference: McKinley et al. (1997) [60]; Warey et al. (2012) [38]; Salvi et al. (2013) [61]; Prabhakar and Boehman (2013) [27]; Abarham et al. (2013) [34]; Li et al. (2014) [62]; Hoseiniet al. (2016) [63]; Razmavar and Malayeri (2016) [64]; Paz et al. (2019) [40]; Luja'n et al. (2019) [42]; Razmavar and Malayeri (2019) [23]; Razmavar et al. (2021) [12]; Han et al. (2023) [25]).

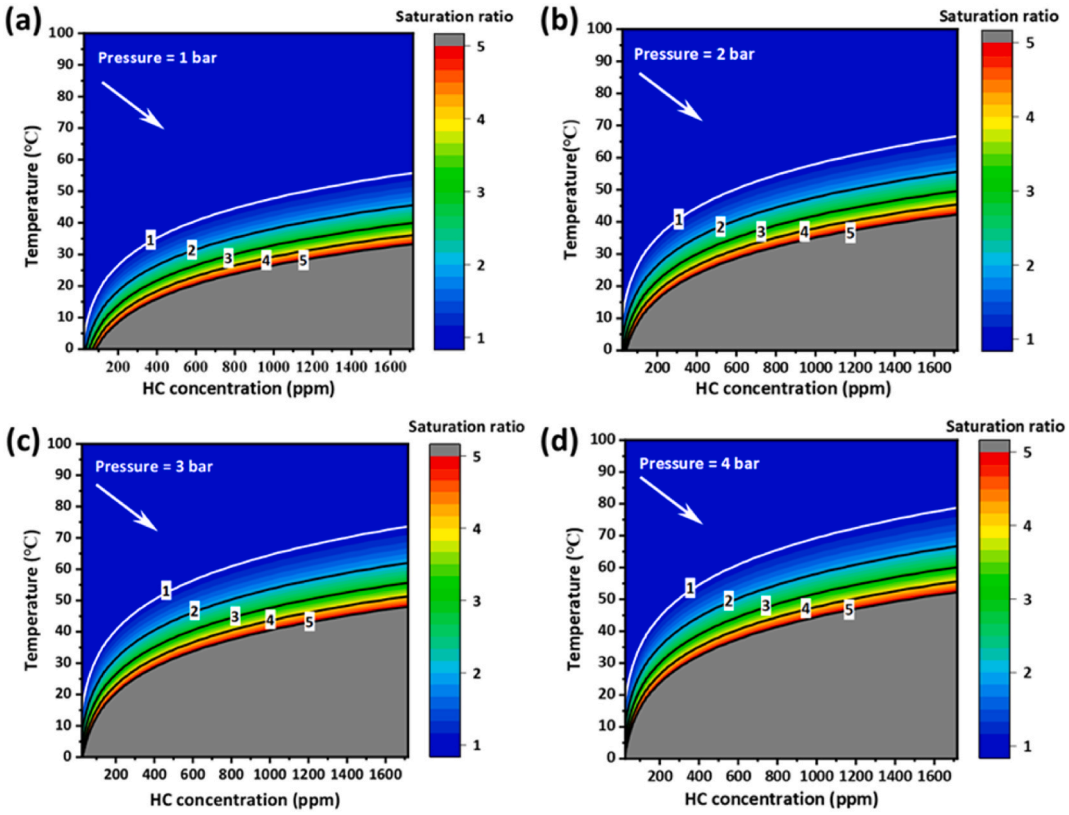

Fig. 4. Saturation ratio distribution map of C12. (a) 1 bar, (b) 2 bar, (c) 3 bar, (d) 4 bar.

temperature and HC concentration at different pressures. The macroscopic distribution of saturation ratios can be divided into three regions: a pure blue region with saturation ratios less than 1, the color gradient region with saturation ratios from 1 to 5, and a gray region with saturation ratios greater than 5. The white arrows in the figure indicate the direction of saturation ratio increase. It can increase with decreasing temperature and increasing HC concentration, which is the direction of HC condensation enhancement. In addition, with the rise of pressure, the color gradient and gray areas move towards the blue area. For example, the white demarcation line at a saturation ratio of 1, this line keeps moving in the direction of higher temperatures and lower HC concentrations as the pressure increases, *i.e.*, in the opposite direction of the white arrows, meaning that HC can achieve equivalent saturation ratios at higher pressures, *i.e.*, equal condensation, at higher temperatures or lower HC concentrations.

The saturation ratios of the HC for the other representative carbon numbers follow the same patterns, as shown in Figs. 5–7. A comparison of the saturation ratio distributions for the different carbon numbers reveals that for the same HC concentrations and pressures, the line with saturation ratios from 1 to 5 moves to a higher temperature region as the number of carbons increases as

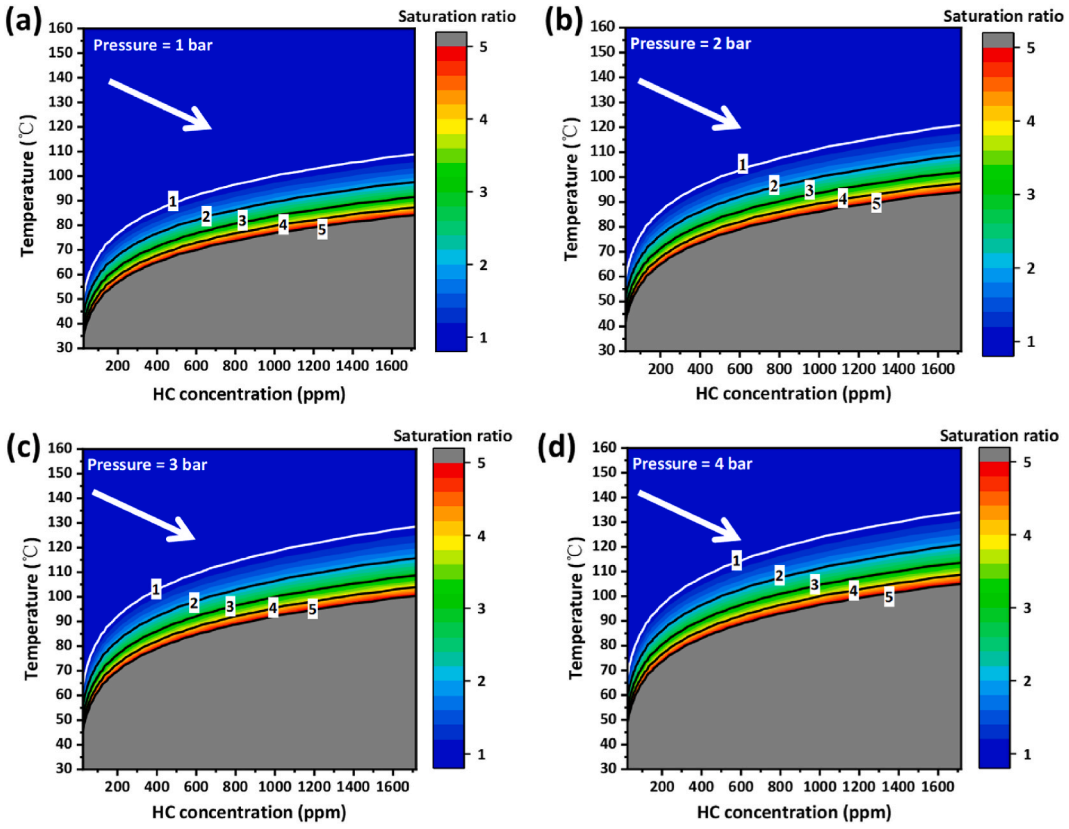

Fig. 5. Saturation ratio distribution map of C16. (a) 1 bar, (b) 2 bar, (c) 3 bar, (d) 4 bar.

expected. Also, using the white line as an example, the line with a saturation ratio of 1 moves to a higher temperature and lower HC concentration region as the carbon number increases, indicating that more carbon numbers (longer carbon chains) can achieve equivalent saturation ratios, *i.e.*, equal degrees of condensation, at higher temperatures and lower HC concentrations.

3.3. Onset temperature distribution map

The transformation from Eq. (1) leads to Eq. (5) as follows:

$$P_{sat}(T) = \frac{P_v}{SR} \tag{5}$$

The partial pressure P_v is a function of the total pressure and HC concentration, while the saturation ratio SR can be used to discriminate the condensation temperatures onset for wall condensation, heterogeneous nucleation, and homogeneous nucleation at SR of 1, 1.5, and 3, respectively, according to the results of the analysis in Section 2.1; and P_{sat} is a function of the carbon number and the temperature; in other words, by setting SR to 1, 1.5 and 3, the distribution of the condensation temperatures onset for the three condensation modes can be obtained under different conditions of total pressure, HC concentration and carbon number.

Figs. 8–10 show the distribution of onset temperatures for wall condensation, heterogeneous nucleation, and homogeneous nucleation, respectively. For the full range of boundary conditions with carbon numbers from 12 to 24, concentrations from 25 to 1717 ppm, and pressures from 1 to 4 bar, Fig. 8 shows that the onset temperatures for wall condensation range from 4 to 218 °C, Fig. 9 shows that the onset temperatures for heterogeneous nucleation range from 1 to 209 °C. Finally, Fig. 10 shows that the onset temperatures for homogeneous nucleation range from −6 to 195 °C (areas below 0 °C are not shown to standardize the vertical scale for comparison).

First, we scrutinized the consistency of the results of the map and past studies to verify the plausibility of the map. The results are shown in the last column of Table 1. Although the boundary conditions of some studies are incomplete and half of them are missing pressure values, assuming that their pressure distributions are in the innermost 1.0 to 2.0 interval, the results show that most of the results of the studies match with the map. The map graphs support that the same results are obtained under the same boundary conditions, and in particular, the results obtained by experimental methods and the results of the map are a perfect match. This map is not currently applicable to the four studies, which may be due to the differences in the used Antoine coefficients in the studies that have been revised over time [65–68]. Overall, the map has a high degree of confidence and organically unifies the relatively scattered and incompatible results of past studies, providing a global view of the onset temperature distribution over the entire operating range of the EGR cooler for different condensing modes while also obtaining specific values when specific boundary conditions are applied.

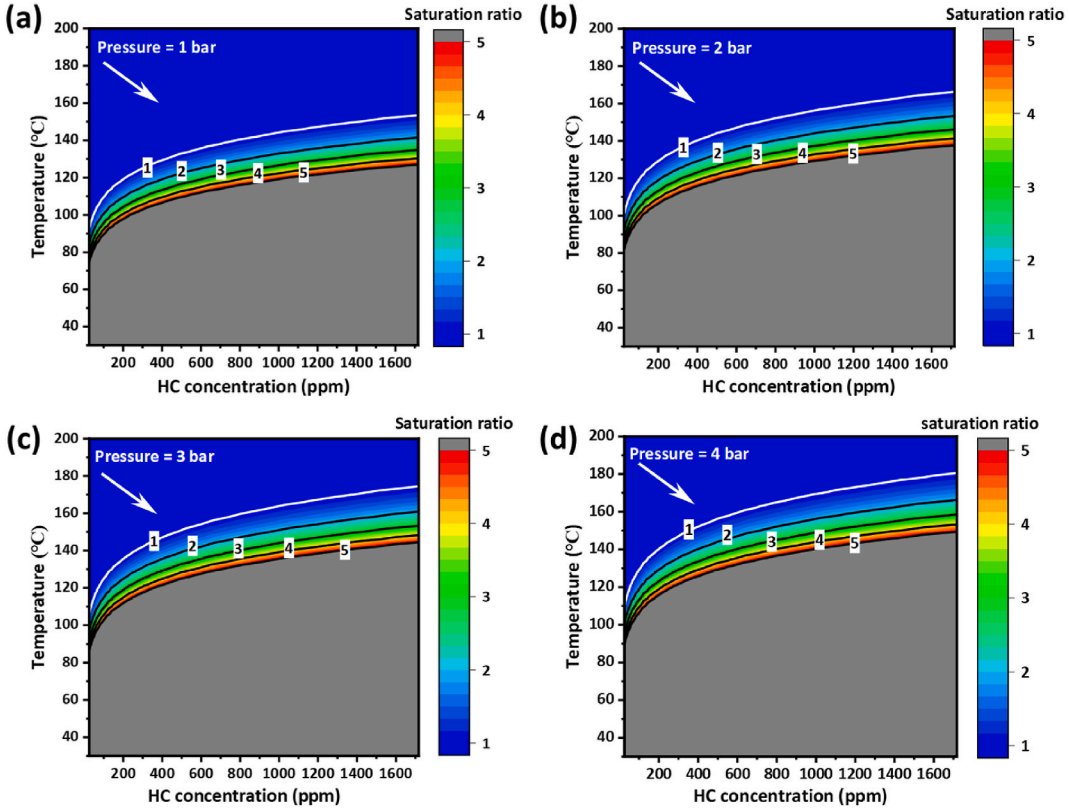

Fig. 6. Saturation ratio distribution map of C20. (a) 1 bar, (b) 2 bar, (c) 3 bar, (d) 4 bar.

Figs. 8–10 also show that the macroscopic trends in the effects of the parameter influences (carbon number, concentration, pressure) are similar on the onset temperatures of the three condensation methods, with the three red arrows at the top indicating the directionality of the effects. *e.g.* for wall condensation in Fig. 8, the onset temperatures of condensation for C12, C16, C20, and C24 are 18 °C, 68 °C, 110 °C, and 143 °C, respectively, for HC concentrations of 100 ppm, and pressures of 1 bar, as indicated by the red star in the figure. The onset temperatures of C24 at 100 ppm, 500 ppm, 900 ppm and 1300 ppm HC in 1 bar are 143 °C, 168 °C, 178 °C and 185 °C, respectively, as indicated by the red crosses. When C24 concentration reaches 100 ppm, the onset temperatures at 1 bar, 2 bar, 3 bar, and 4 bar are 143 °C, 153 °C, 159 °C, and 164 °C, respectively, as shown by the red triangles in figure. As the carbon number N increases, the HC concentration C increases, and the pressure P increases, the onset temperature of condensation increases for all three types.

More importantly, the cooling temperature of 90 °C is a reference line for the cooler during regular operation. For C12, the onset temperature for all three condensation methods are less than 90 °C, which means that no C12 condensation occurs in the cooler; for C16, the portion of the cooler above the 90 °C reference line has higher onset temperature, which implies that C16 condenses under these boundary conditions, while the portion below the 90 °C reference line does not. Similarly, for C20, both wall condensation and heterogeneous nucleation occur, and homogeneous nucleation occurs only at low HC concentrations (from 25 to 50 ppm) and low pressures (from 1 to 2 bar), and for C24, all three modes of condensation occur. The onset temperatures of all three are much higher than those for C24. Even at HC concentrations as low as 25 ppm, the onset temperature for all three types of condensation is well above 90 °C.

3.4. Sensitivity analysis

Based on the orthogonal design of Table 3, the onset temperature corresponding to the three HC condensation methods is calculated separately, and the results are shown in Table 4.

Tables 5, 6 and 7 shows the results of the analysis of variance (ANOVA) for the three different condensation methods, df refers to the degree of freedom, and F refers to the F statistic. Results shows that the order of influence of the parameters on the condensation point temperature is carbon number > concentration > pressure. The Prob value is less than the set significance level of 0.05, which re-confirms that carbon number, concentration, and pressure significantly affect the onset temperature.

Fig. 11 shows the contribution of carbon number, HC concentration, and pressure to the onset temperature for the three condensation methods. Carbon number has the most significant contribution, followed by HC concentration and pressure. More specifically, the contributions of carbon number were 0.78, 0.79, and 0.82 for wall condensation, heterogeneous nucleation, and homogeneous nucleation, respectively; HC concentration was 0.20, 0.19, and 0.17 for wall condensation, heterogeneous nucleation,

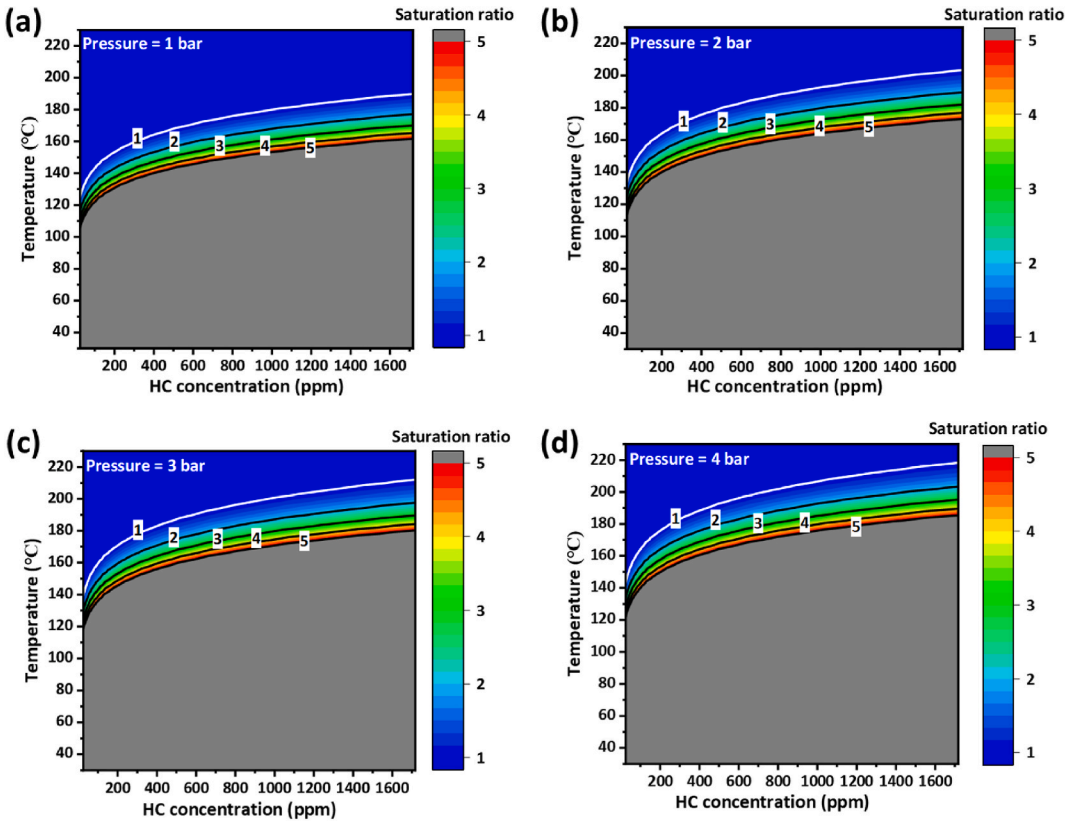

Fig. 7. Saturation ratio distribution map of C24. (a) 1 bar, (b) 2 bar, (c) 3 bar, (d) 4 bar.

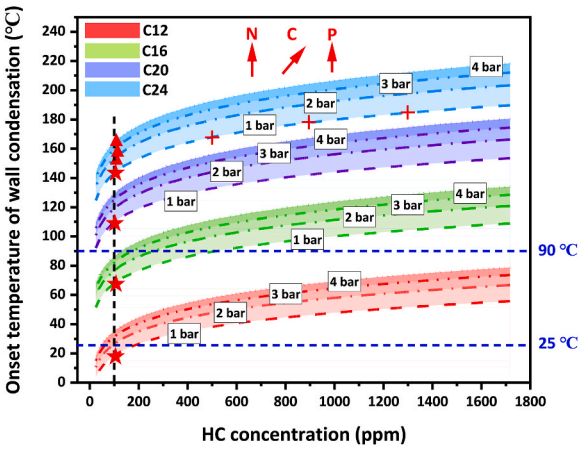

Fig. 8. Onset temperature distribution map of HC wall condensation.

and homogeneous nucleation, respectively; and pressure was 0.02, 0.02, and 0.01 for wall condensation, heterogeneous nucleation, and homogeneous nucleation, respectively. It can be seen that, the contribution rate of the three parameters is at the same level in all three condensation modes.

3.5. Discussion

EGR coolers are optimized for broader operating ranges, faster response times, more precise fluid properties (temperature, flow rate, pressure, etc.), higher thermal efficiency, lower pressure drop, and better fouling resistance. The Euro 7 standard, which is to be implemented, emphasizes the need for a wider operating range and more precise fluid control, which is strongly dependent on the interaction of the exhaust gases and the cooler, in particular the occurrence and intensity of HC condensation. The latter highly

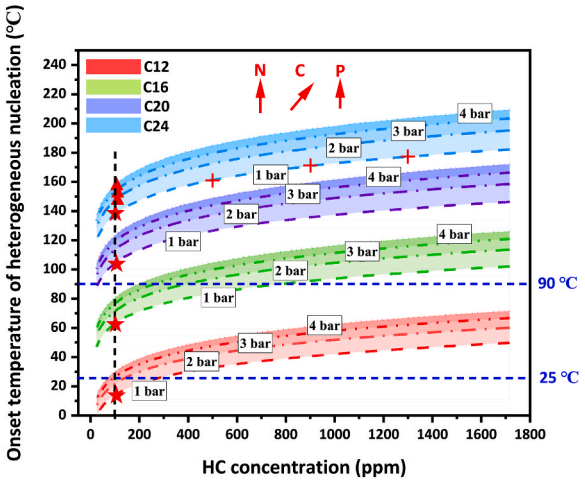

Fig. 9. Onset temperature distribution map of HC heterogeneous nucleation.

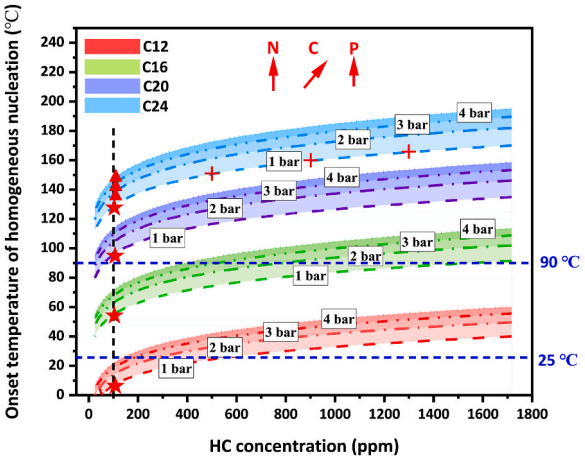

Fig. 10. Onset temperature distribution map of HC homogeneous nucleation.

Table 4
Results of the orthogonal array of L16(4^3).

Program	Carbon number	Concentration (ppm)	Pressure (bar)	Onset temperature (°C)		
				Wall condensation	Heterogeneous nucleation	Homogeneous nucleation
①	12	25	1	3.6	−0.7	−6.7
②	12	589	2	49.8	44.2	34.8
③	12	1153	3	66.9	60.2	49.7
④	12	1717	4	78.7	71.5	60.1
⑤	16	589	1	91.6	85.6	76.1
⑥	16	25	2	59.2	54.5	46.9
⑦	16	1717	3	128.4	120.9	108.7
⑧	16	1153	4	126.3	118.8	106.8
⑨	20	1153	1	146.2	139.6	128.4
⑩	20	1717	2	166.3	158.6	146.1
⑪	20	25	3	105.5	100.3	91.9
⑫	20	589	4	159.1	151.7	139.6
⑬	24	1717	1	189.7	182.1	169.9
⑭	24	1153	2	195.3	187.5	174.8
⑮	24	589	3	190.1	182.4	170.4
⑯	24	25	4	142.8	137.3	128.0

Table 5
The ANOVA for the onset temperature of wall condensation.

Results of ANOVA under wall condensation					
Source	df	S	Mean S	F	Prob > F
Carbon number	3	37607.8	12535.9	747.16	0
Concentration	3	9686.4	3228.8	198.31	0
Pressure	3	804.2	268.1	15.98	0.0029

Table 6
The ANOVA for the onset temperature of heterogeneous nucleation.

Results of ANOVA under wall condensation					
Source	df	S	Mean S	F	Prob > F
Carbon number	3	36935	12311.7	863.08	0
Concentration	3	8848.1	2949.4	206.76	0
Pressure	3	738	246	17.25	0.0018

Table 7
The ANOVA for the onset temperature of homogeneous nucleation.

Results of ANOVA under wall condensation					
Source	df	S	Mean S	F	Prob > F
Carbon number	3	35662.4	11887.5	919.62	0
Concentration	3	7650.3	2550.1	197.28	0
Pressure	3	626.6	208.9	16.16	0.0038

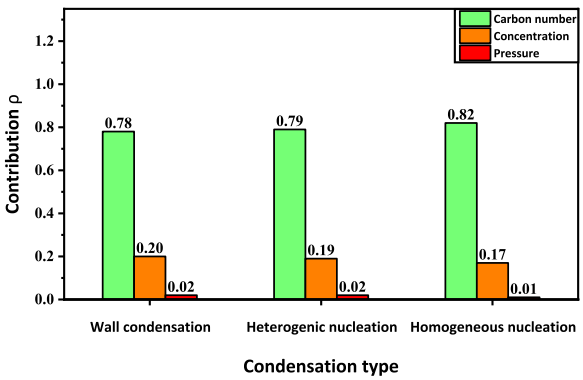

Fig. 11. Contribution of each factor for HC condensation onset temperature.

influences the thermodynamic and kinetic parameters of the exhaust gases at the outlet of the cooler, and which are visualized by the maps mentioned above of the saturation ratios and the condensation onset temperatures.

Based on the results of the onset temperature map and sensitivity analysis, if optimized with the dual objective of further reducing the exhaust gas outlet temperature and avoiding HC condensation, the decisive factor is the carbon number, especially the HC with long carbon chains (≥C20), which is possible to achieve if it is possible to inhibit their presence and/or to keep the HC concentration within a specific range. Suppose a broader range of EGR operation and condensation avoidance is optimized as a dual objective. In that case, the more comprehensive range here mainly refers to expanding the application of EGR technology to the start-up phase or low-temperature scenarios, a significant trade-off problem. However, the potential for expansion into the low temperature region is still substantial if the long carbon chain HC can be cut out. If optimizing for a higher EGR rate and avoiding HC condensation is the dual objective, increasing the exhaust gas pressure may be feasible, and its effect on the onset temperature is minimal, and a slight temperature gain is acceptable. The development of the EGR cooler operation strategy is a systematic project, which needs to be a trade off between the power performance and the emission properties and the synergistic matching of the exhaust system, supercharger, and intake system; the feasibility of the above proposal needs further verification.

Based on the above analysis, practical implications for engine system design are minimize engine-out HC levels, minimize soot concentration. An oxidation catalyst between the engine and the cooler might reduce HC levels and therefore fouling. In some operating conditions, even a small reduction in HC concentration can have a large effect on condensation amount.

4. Conclusion

Under the conditions of the influencing parameters being HC species C12 to C25, concentration from 25 to 1717 ppm, and pressure from 1 to 4 bar, the present work systematically dissects the distribution of HC condensation onset temperatures in the EGR cooler, and the following conclusions can be drawn.

(i) The HC condensation onset temperature maps have broad applicability and strong practicality, considering both macroscopic qualitative and microscopic quantitative properties.
(ii) HC condensation onset temperature can exceed 200 °C of temperature difference depending on the working conditions, with the most extreme low and high temperatures being −6 °C and 218 °C, respectively.
(iii) This HC condensation onset temperature map still has some limitations, and future enhancements could be considered in terms of a more accurate saturation ratio criterion, a richer set of HC species (HC compounds other than n-alkanes), and more realistic interactions internal the system, including those with particulate matter, other non-condensable gases, and the cooler.
(iv) To avoid HC condensation in the EGR cooler, it is essential to primarily control hydrocarbons with long carbon chains, especially those above C20.

CRediT authorship contribution statement

Zhiqiang Han: Writing – review & editing, Validation, Investigation. **Liping Luo:** Writing – original draft, Visualization, Software, Investigation, Formal analysis. **Yipeng Yao:** Writing – review & editing, Visualization, Supervision, Project administration, Methodology, Conceptualization. **Hai Du:** Writing – review & editing, Visualization. **Wei Tian:** Visualization, Investigation, Formal analysis. **Xueshun Wu:** Writing – review & editing, Software. **Marie-Eve Duprez:** Writing – review & editing. **Guy De Weireld:** Writing – review & editing, Supervision.

Declaration of competing interest

The authors declare that they have no known competing financial interests or personal relationships that could have appeared to influence the work reported in this paper.

Data availability

Data will be made available on request.

Acknowledgments

The work is jointly funded the National Defense Science and Technology Key Laboratory Fund Project [2022-JCJQ-LB-062-0102], the National Natural Science Foundation of China [51776177, 51876145]. Yipeng Yao acknowledges the China Scholarship Council (CSC) [202208510023], Wallonie-Bruxelles International (WBI), and Belgium National Fund of Fonds de la Recherche Scientifique–FNRS (F.R.S.-FNRS) for their financial support.

References

[1] M.A. GóMEZ, R. MartíN, S. Chapela, et al., Steady CFD combustion modeling for biomass boilers: an application to the study of the exhaust gas recirculation performance, Energy Convers. Manag. 179 (2019) 91–103.
[2] P. Grajetzki, T. Onda, H. Nakamura, et al., Investigation of the chemical and dilution effects of major EGR constituents on the reactivity of PRF by weak flames in a micro flow reactor with a controlled temperature profile, Combust. Flame 209 (2019) 13–26.
[3] K. AL-Qurashi, A.D. Lueking, A.L. Boehman, The deconvolution of the thermal, dilution, and chemical effects of exhaust gas recirculation (EGR) on the reactivity of engine and flame soot, Combust. Flame 158 (9) (2011) 1696–1704.
[4] A.C.T. Malaquias, N.A.D. Netto, R.B.R. Da Costa, et al., Combined effects of internal exhaust gas recirculation and tumble motion generation in a flex-fuel direct injection engine, Energy Convers. Manag. 217 (2020) 113007.
[5] M.C. Mulenga, D.K. Chang, J.S. Tjong, et al., Diesel EGR cooler fouling at freeway cruise, SAE Technical Paper (2009).
[6] N. Ladommatos, S.M. Abdelhalim, H. Zhao, et al., The dilution, chemical, and thermal effects of exhaust gas recirculation on diesel engine emissions-Part 4: effects of carbon dioxide and water vapour, SAE Trans. (1997) 1844–1862.
[7] N. Ladommatos, S. Abdelhalim, H. Zhao, et al., The Dilution, Chemical, and Thermal Effects of Exhaust Gas Recirculation on Diesel Engine Emissions-Part 3: Effects of Water Vapour, 1997. SAE Technical Paper.
[8] E. Gumus, M. Otkur, Design of an optimum compact EGR cooler in a heavy-duty diesel engine towards meeting Euro 7 emission regulations, Sustainability 15 (16) (2023).
[9] DIESELNET, European Commission Proposes Euro 7/VII Emission Standards [Z], 2022.
[10] H.E.F. Cleaning, Heat Exchanger Fouling & Cleaning Conference Series [Z], 2023.
[11] K. Hooman, M.R. Malayeri, Metal foams as gas coolers for exhaust gas recirculation systems subjected to particulate fouling, Energy Convers. Manag. 117 (2016) 475–481.
[12] A. Razmavar, M.R. Malayeri, M.S. Abd-Elhady, Influence of secondary flow on the thermal performance of exhaust gas recirculation (EGR) coolers, Int. J. Therm. Sci. 161 (2021) 106720.
[13] C. Paz, E. SuáREZ, J. Vence, et al., Fouling evolution on ribbed surfaces under EGR dry soot conditions: experimental measurements and 3D model validation, Int. J. Therm. Sci. (2020) 151.
[14] A. Khoshnood, M. Maerefat, G. Imani, et al., Effect of soot particle deposition on porous fouling formation and thermal characteristics of an exhaust gas recirculation cooler, Appl. Therm. Eng. 229 (2023) 120629.
[15] S.-Y. Wu, Y. Chen, Y.-R. Li, et al., The effect of fouling on thermodynamic performance of forced convective heat transfer through a duct, Energy Convers. Manag. 48 (8) (2007) 2399–2406.

[16] F. Pelella, L. Viscito, A.W. Mauro, Soft faults in residential heat pumps: possibility of evaluation via on-field measurements and related degradation of performance, Energy Convers. Manag. 260 (2022) 115646.
[17] M.H. Pourrezaei, M.R. Malayeri, K. Hooman, Thermal performance and mechanisms of soot deposition in foam structured exhaust gas recirculation coolers, Int. J. Therm. Sci. (2019) 146.
[18] K.H. Yoo, J. Hoard, A. Boehman, et al., Experimental Studies of EGR Cooler Fouling on a GDI Engine, SAE Technical Paper, 2016, 2016-April.
[19] Y. Bravo, C. Arnal, C. Larrosa, et al., Impact on Fouling of Different Exhaust Gas Conditions with Low Coolant Temperature for a Range of EGR Cooler Technologies, SAE Technical Paper, 2018, 2018-April.
[20] B. Prabhakar, Examination of EGR Cooler Fouling and Engine Efficiency Improvement in Compression Ignition Engines [D], The Pennsylvania State University, 2013.
[21] M.J. Lance, H. Bilheux, J.-C. Bilheux, et al., Neutron tomography of exhaust gas recirculation cooler deposits, SAE Technical Paper 1 (2014).
[22] Y. Yao, Z. Han, W. Tian, et al., Three condensation paths of exhaust and its five effects on exhaust gas recirculation (EGR) cooler fouling and thermal performance: a review, Case Stud. Therm. Eng. 47 (2023) 103099.
[23] A. Razmavar, M.R. Malayeri, Thermal performance of a rectangular exhaust gas recirculation cooler subject to hydrocarbon and water vapor condensation, Int. J. Therm. Sci. 143 (2019) 1–13.
[24] D. Styles, E. Curtis, N. Ramesh, et al., Factors impacting EGR cooler fouling - main effects and interactions, in: 16th Directions in Engine-Efficiency and Emission Research Conference (DEER). Detroit, MI, 2010, pp. 1–25.
[25] Z. Han, Y. Yao, W. Tian, et al., Effect of hydrocarbon condensation on fouling and heat exchange efficiency in EGR cooler, Int. J. Therm. Sci. 184 (2023) 12.
[26] C. Paz, M. Conde, J. Vence, et al., Experimental Study of the Effect of Hydrocarbon Condensation on the Fouling Deposits of Exhaust Gas Recirculation Coolers; Proceedings of the Heat Exchanger Fouling and Cleaning – 2019, F, 2019 [C].
[27] B. Prabhakar, A.L. Boehman, Effect of engine operating conditions and coolant temperature on the physical and chemical properties of deposits from an automotive exhaust gas recirculation cooler, J. Eng. Gas Turbines Power 135 (2) (2013).
[28] S. Liebsch, M. Leesch, P. Zumpf, et al., EGR Cooler Fouling Reduction: A New Method for Assessment in Early Engine Development Phase, 2022. SAE Technical Paper.
[29] C. Paz, E. SuáREZ, J. Vence, et al., Evolution of EGR cooler deposits under hydrocarbon condensation: analysis of local thickness, roughness, and fouling layer density, Int. J. Therm. Sci. (2021) 161.
[30] M.J. Lance, Z.G. Mills, J.C. Seylar, et al., The effect of engine operating conditions on exhaust gas recirculation cooler fouling, Int. J. Heat Mass Tran. 126 (2018) 509–520.
[31] X. Zhang, W. Tian, J. Li, et al., Effects of coolant temperature on particulate deposition and cooling efficiency of EGR coolers, J. Mech. Sci. Technol. 35 (7) (2021) 3231–3237.
[32] J. Li, X. Zhang, H. Wu, et al., Effect of hydrocarbon concentration on particulate deposition and microstructure of the deposit in exhaust gas recirculation cooler, Int. J. Automot. Technol. 23 (3) (2022) 775–784.
[33] M. Abarham, J. Hoard, D.N. Assanis, et al., Modeling of thermophoretic soot deposition and hydrocarbon condensation in EGR coolers, SAE International Journal of Fuels and Lubricants 2 (1) (2009) 921–931.
[34] M. Abarham, T. Chafekar, J.W. Hoard, et al., In-situ visualization of exhaust soot particle deposition and removal in channel flows, Chem. Eng. Sci. 87 (2013) 359–370.
[35] K. Tanaka, K. Hiroki, T. Kikuchi, et al., Investigation of mechanism for formation of EGR deposit by in situ ATR-FTIR spectrometer and SEM, SAE International Journal of Engines 9 (4) (2016) 2242–2249.
[36] C.S. Sluder, J.M.E. Storey, S.A. Lewis, et al., Hydrocarbons and particulate matter in EGR cooler deposits: effects of gas flow rate, coolant temperature, and oxidation catalyst, SAE International Journal of Engines 1 (1) (2008) 1196–1204.
[37] A.S. Bika, A. Warey, D. Long, et al., Characterization of soot deposition and particle nucleation in exhaust gas recirculation coolers, Aerosol. Sci. Technol. 46 (12) (2012) 1328–1336.
[38] A. Warey, S. Balestrino, P. Szymkowicz, et al., A one-dimensional model for particulate deposition and hydrocarbon condensation in exhaust gas recirculation coolers, Aerosol. Sci. Technol. 46 (2) (2012) 198–213.
[39] A. Warey, D. Long, S. Balestrino, et al., Visualization and Analysis of Condensation in Exhaust Gas Recirculation Coolers, 2013. SAE Technical Paper.
[40] C. Paz, E. SuáREZ, J. Vence, et al., CFD Study of the Fouling Layer Evolution Due to Soot Deposition and Hydrocarbon Condensation inside an Exhaust Gas Recirculation Cooler; Proceedings of the Heat Exchanger Fouling and Cleaning – 2019, F, 2019 [C].
[41] J. Galindo, V. Dolz, J. Monsalve-Serrano, et al., Advantages of using a cooler bypass in the low-pressure exhaust gas recirculation line of a compression ignition diesel engine operating at cold conditions, Int. J. Engine Res. 22 (5) (2020) 1624–1635.
[42] J.M. LuJáN, V. Dolz, J. Monsalve-Serrano, et al., High-pressure exhaust gas recirculation line condensation model of an internal combustion diesel engine operating at cold conditions, Int. J. Engine Res. 22 (2) (2019) 407–416.
[43] W. Hinds, in: Aerosol Technology: Properties, Behavior, and Measurement of Airborne Particles 2nd, John Wiley & Sons, New York, 1999.
[44] P.J. Wlasits, R. Konrat, P.M. Winkler, Heterogeneous nucleation of supersaturated water vapor onto sub-10 nm nanoplastic particles, Environ. Sci. Technol. 57 (4) (2023) 1584–1591.
[45] L. Nichman, M. Wolf, P. Davidovits, et al., Laboratory study of the heterogeneous ice nucleation on black-carbon-containing aerosol, Atmos. Chem. Phys. 19 (19) (2019) 12175–12194.
[46] C. Tauber, G. Steiner, P.M. Winkler, Counting efficiency determination from quantitative intercomparison between expansion and laminar flow type condensation particle counter, Aerosol. Sci. Technol. 53 (3) (2019) 344–354.
[47] A. Kupc, P.M. Winkler, A. Vrtala, et al., Temperature dependence of heterogeneous nucleation of water vapor on Ag and NaCl particles; proceedings of the, in: AIP Conference Proceedings, Fort Collins, Colorado, USA, F, AIP, 2013 [C].
[48] I.A. Khalek, D.B. Kittelson, F. Brear, Nanoparticle Growth during Dilution and Cooling of Diesel Exhaust: Experimental Investigation and Theoretical Assessment, F, 2000 [C].
[49] M. Dong, Y. Li, D. Song, et al., Uncertainty and global sensitivity analysis of levelized cost of energy in wind power generation, Energy Convers. Manag. 229 (2021) 113781.
[50] R. Fan, G. Chang, Y. Xu, et al., Investigating and quantifying the effects of catalyst layer gradients, operating conditions, and their interactions on PEMFC performance through global sensitivity analysis, Energy 290 (2024) 130128.
[51] A. Chuat, C. Terrier, J. Schnidrig, et al., Identification of typical district configurations: a two-step global sensitivity analysis framework, Energy 296 (2024) 131116.
[52] J. Vence, C. Paz, E. SuáREZ, et al., Analysis of the local growth and density evolution of soot deposits generated under hydrocarbon condensation: 3D simulation and detailed experimental validation, Results in Engineering 18 (2023) 101166.
[53] S. Sakaida, S. Kimiyama, T. Sakai, et al., Effect of Exhaust Gas Composition on EGR Deposit Formation, 2019. SAE Technical Paper.
[54] K. Tanaka, T. Sakai, T. Fujino, et al., Evaluation of mechanism for EGR deposit formation based on spatially- and time-resolved scanning-electron-microscope observation, SAE International Journal of Advances and Current Practices in Mobility 3 (1) (2020) 150–158.
[55] K. Kinoshita, Y. Takeda, Y. Abe, et al., Elucidation of exhaust gas recirculation deposit formation mechanism based on chemical analysis of components, Fuel 337 (2023) 127197.
[56] Y. Bravo, J. Lujan, A. Tiseira, Characterization of EGR cooler response for a range of engine conditions, SAE International Journal of Engines 6 (1) (2013) 587–595.
[57] C.S. Sluder, J.M. Storey, M.J. Lance, Effectiveness Stabilization and Plugging in EGR Cooler Fouling, 2014. SAE Technical Paper.
[58] Y. Bravo, C. Larrosa, J. Lujan, et al., Evaluation of EGR System Implementation in a GTDI Engine with Different Configurations: Assessment on Fouling and Corrosion Issues, 2016, https://doi.org/10.4271/2016-01-1016. SAE Technical Paper.

[59] Y. Yao, Z. Han, W. Tian, et al., An original nondestructive sampling method to study the effect of gravity on the deposition of micron-sized large particles in exhaust gas recirculation (EGR) cooler fouling, Int. J. Engine Res. 25 (5) (2023) 928–939.
[60] T. Mckinley, Modeling Sulfuric Acid Condensation in Diesel Engine EGR Coolers, SAE International, 1997, https://doi.org/10.4271/970636. SAE Technical Paper Series.
[61] A.A. Salvi, J. Hoard, P.K. Jagarlapudi, et al., Optical and Infrared In-Situ Measurements of EGR Cooler Fouling; Proceedings of the SAE Technical Paper, F, 2013 [C].
[62] H. Li, J. Hoard, D. Styles, et al., Visual Study of In-Situ EGR Cooler Fouling Layer Evolution; Proceedings of the Volume 1: Large Bore Engines; Fuels; Advanced Combustion; Emissions Control Systems, Columbus, Indiana, USA, F, American Society of Mechanical Engineers, 2014.
[63] S.S. Hoseini, G. Najafi, B. Ghobadian, Experimental and numerical investigation of heat transfer and turbulent characteristics of a novel EGR cooler in diesel engine, Appl. Therm. Eng. 108 (2016) 1344–1356.
[64] A. Reza Razmavar, M. Reza Malayeri, A simplified model for deposition and removal of soot particles in an exhaust gas recirculation cooler, J. Eng. Gas Turbines Power 138 (1) (2016).
[65] C.L. Yaws, P.K. Narasimhan, C. Gabbula, Yaws' Handbook of Antoine Coefficients for Vapor Pressure, 2005. Knovel Norwich, NY.
[66] C.L. Yaws, The Yaws Handbook of Vapor Pressure: Antoine Coefficients [M], Elsevier Science, 2007.
[67] C.L. Yaws, P. Narasimhan, C. Gabbula, Online version available at:, in: Yaws' Handbook of Antoine Coefficients for Vapor Pressure, 2nd Electronic Edition, 2009.
[68] C.L. Yaws, in: The Yaws Handbook of Vapor Pressure: Antoine Coefficients, second ed., Gulf Professional Publishing, 2015.